How to cite: *Angew. Chem. Int. Ed.* **2021**, *60*, 23722–23728
International Edition: doi.org/10.1002/anie.202106398
German Edition: doi.org/10.1002/ange.202106398

VIP **Luminescence** *Very Important Paper*

A Near-Infrared-II Emissive Chromium(III) Complex

Narayan Sinha, Juan-Ramón Jiménez, Björn Pfund, Alessandro Prescimone, Claude Piguet, and Oliver S. Wenger**

Abstract: *The combination of π-donating amido with π-accepting pyridine coordination units in a tridentate chelate ligand causes a strong nephelauxetic effect in a homoleptic Cr^{III} complex, which shifts its luminescence to the NIR-II spectral range. Previously explored Cr^{III} polypyridine complexes typically emit between 727 and 778 nm (in the red to NIR-I spectral region), and ligand design strategies have so far concentrated on optimizing the ligand field strength. The present work takes a fundamentally different approach and focusses on increasing metal–ligand bond covalence to shift the ruby-like ^2E emission of Cr^{III} to 1067 nm at 77 K.*

Introduction

Chromium(III) complexes played a central role in the development of coordination chemistry, and nowadays serve as textbook examples of substitution-inert compounds with rich optical spectroscopic and magnetic properties.[1] Many Cr^{3+} containing materials show photo-luminescence in the solid state,[2] and carefully designed molecular complexes of Cr^{III} emit in solution at room temperature. However, under these latter conditions the luminescence quantum yields (φ) of classical polypyridine complexes such as those in Figure 1 a–c are typically on the order of 0.1 % or lower.[3]

For the recently disclosed $[Cr(ddpd)_2]^{3+}$ complex (Figure 1 d),[5,7] φ-values up to 30 % were achievable in solution,[8] and this represented a quantum leap for the photophysics of molecular Cr^{III} compounds. The ability of ddpd to chelate Cr^{III} with significantly larger bite angles than the ligands in Figure 1 a–c is a key factor contributing to the favorable luminescence behavior of $[Cr(ddpd)_2]^{3+}$, and a similar concept was later exploited with the tridentate dqp ligand (Figure 1 e).[6,9] The nearly ideal octahedral coordination of Cr^{III} by ddpd and dqp implies strong spatial overlaps between the spectroscopically relevant metal 3d- and ligand-orbitals, resulting in a strong ligand field created by the π-acceptor units pyridine and quinoline. As the coordination environments of $[Cr(ddpd)_2]^{3+}$ and $[Cr(dqp)_2]^{3+}$ deviate only relatively little from O_h symmetry, undesirable splitting of degenerate excited states by symmetry lowering (such as the case for example in the trigonally distorted $[Cr(phen)_3]^{3+}$ complex) can be kept minimal. These combined effects of high symmetry and strong ligand field are helpful, because they increase the energy gap between the emissive ^2E and the higher-lying $^4T_2$ state (Figure 2 a), thereby diminishing the thermal population of the latter (via reverse intersystem crossing) and minimizing nonradiative relaxation from the strongly distorted $^4T_2$ excited state. The enhancement of ligand field strength (captured by an increase of the parameter 10 Dq) predominantly acts on the $^4T_2$ energy, but affects

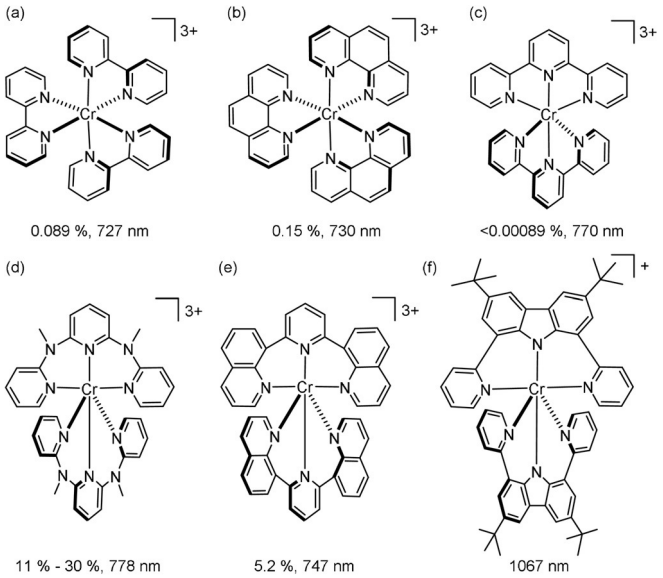

Figure 1. Molecular structures of (a) $[Cr(bpy)_3]^{3+}$ (bpy = 2,2′-bipyridine),[3b,4] (b) $[Cr(phen)_3]^{3+}$ (phen = 1,10-phenanthroline),[3b,4] (c) $[Cr(tpy)_2]^{3+}$ (tpy = 2,2′:6′,2″-terpyridine),[3b,4] (d) $[Cr(ddpd)_2]^{3+}$ (ddpd = N,N′-dimethyl-N,N′-dipyridine-2-yl-2,6-diamine),[5] and (e) $[Cr(dqp)_2]^{3+}$ (dqp = 2,6-di(quinoline-8-yl)pyridine)[6] along with their luminescence quantum yields (φ) in solution at room temperature and wavelengths of emission band maxima (λ_{em}). (f) Molecular structure of the new $[Cr(dpc)_2]^+$ complex reported herein (dpc = 3,6-di-*tert*-butyl-1,8-di(pyridine-2-yl)-carbazolato) and its emission peak wavelength.

[*] N. Sinha, B. Pfund, O. S. Wenger
Department of Chemistry, University of Basel
St. Johanns-Ring 19, 4056 Basel (Switzerland)
E-mail: oliver.wenger@unibas.ch
J.-R. Jiménez, C. Piguet
Department of Inorganic and Analytical Chemistry, University of Geneva
30 quai E. Ansermet, 1211 Geneva 4 (Switzerland)
E-mail: claude.piguet@unige.ch
A. Prescimone
Department of Chemistry, University of Basel, BPR 1096
Mattenstrasse 24a, 4058 Basel (Switzerland)
Supporting information and the ORCID identification number(s) for the author(s) of this article can be found under: https://doi.org/10.1002/anie.202106398.

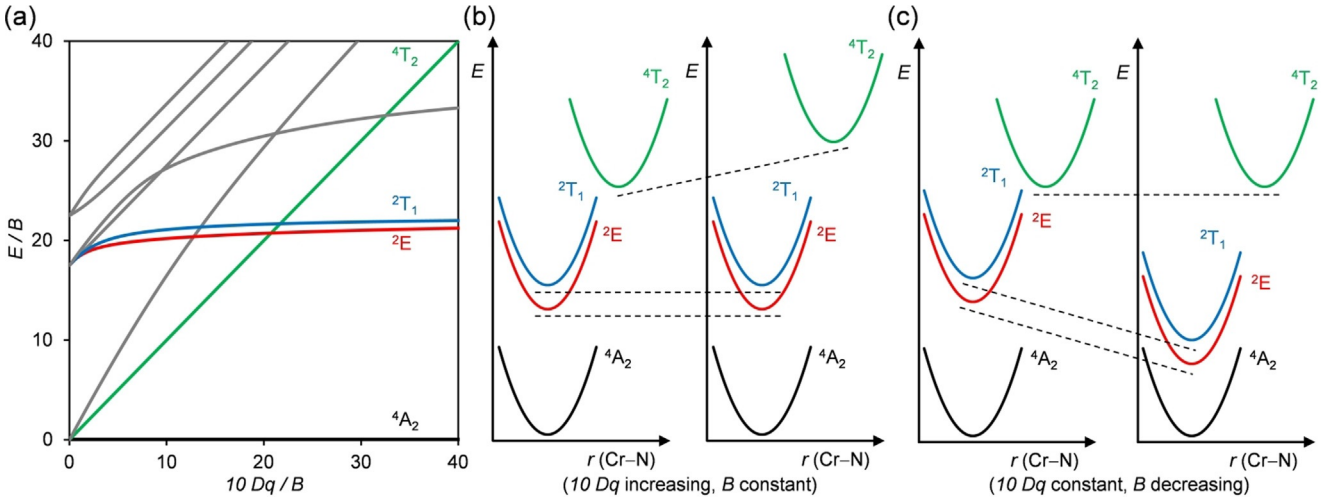

Figure 2. (a) Tanabe–Sugano diagram for the d^3 valence electron configuration in O_h symmetry. Single configurational coordinate diagrams illustrating (b) the influence of an increase in ligand field parameter (10 Dq) on the ^2E, $^2T_1$, and $^4T_2$ energies and (c) the influence of an increase in metal–ligand bond covalence (decrease of Racah B parameter) on the respective energies.

the energy of the ^2E spin-flip transition much less (Figure 2b), and consequently the emission peak wavelengths (λ_{em}) of the Cr^{III} complexes in Figure 1a–e are relatively similar (727–778 nm). In other words, the strategy pursued with the complexes in Figure 1d/e (and its congeners)[5,7–8,10] is highly successful for the optimization of luminescence quantum yields, but it is not well suited for emission color tuning.

The energy of the $^2E \rightarrow {}^4A_2$ spin-flip transition of Cr^{III} is more susceptible to electron-electron repulsion than ligand field strength (Figure 2c). The mutual repulsion between d-electrons is quantified by the Racah *B* parameter, which adopts a value of 918 cm^{-1} for the free Cr^{3+} ion in the gas phase.[11] In coordination environments, the formation of metal–ligand bonds with covalent character leads to the nephelauxetic effect, meaning that d-electrons are spatially more distributed and less confined to the metal core.[12] Consequently, their mutual repulsion diminishes, manifesting in *B*-values on the order of 650–810 cm^{-1} for polypyridine complexes of Cr^{III}. We reasoned that if metal–ligand bond covalence was further increased, the ^2E emission wavelength could possibly be shifted into the NIR-II region beyond 1000 nm. To the best of our knowledge, this has not been achievable yet with molecular Cr^{III} complexes.[13]

NIR emitters have applications in light-emitting devices,[14] fiber-optic telecommunications,[15] anti-counterfeit inks,[16] oxygen sensing,[5,10] bio-sensing and bio-imaging,[17] as well as in night-vision readable displays.[18] Many of the respective luminophores are based on lanthanide complexes[17] or coordination compounds with second- or third-row transition metal elements,[19] whilst others are made from organic dyes or a combination of organic chromophores with precious metal complexes.[20] NIR-II luminescence is particularly advantageous for in vivo imaging, for example to locate malignant tissue due to its deep penetration, high signal to background ratio, and reduced interfering signals.[21] The recent surge of interest in photoactive complexes made from Earth-abundant metals resulted in several compounds emitting in the NIR-I region between 700 and 950 nm,[22] but NIR-II emitters are extremely scarce among base metal complexes so far.[23] Obvious economic advantages can result from the replacement of precious and rare metals by more abundant and cheaper alternatives, but furthermore the question how NIR-II emission can become competitive with undesired excited-state relaxation processes in first-row transition metal complexes is of considerable fundamental interest.[24]

Inspired by recent advances in iron(II) photophysics where the change from classical polypyridine ligands to chelates with amido donors led to a drastically altered electronic structure,[25] we identified the tridentate dpc ligand (Figure 1f) as a promising candidate for Cr^{III} complexes with red-shifted ^2E luminescence. In the earlier Fe^{II} work,[26] so-called "HOMO inversion" was in key focus,[27] whilst here the conceptually much different aspect of increased metal–ligand bond covalence is of central interest. Comprised of a central π-donating amido donor flanked by two σ-donating and π-accepting pyridine units, this chelate can be expected to coordinate Cr^{III} in nearly optimal octahedral fashion,[25,28] hence the design of this ligand takes some of the lessons learned from the coordination bite-angle optimized compounds in Figure 1d/e into account. The key difference to the previously investigated complexes is the presence of an anionic coordination unit, which strongly affects the electron density at the metal. π-donor ligands commonly weaken the ligand field due to energetic destabilization of the metal-based t_{2g}-like orbitals,[29] which is in clear contrast to the design principle of maximizing 10 Dq pursued in recent studies (Figure 1d/e). We speculated that the dpc ligand would enable increased overall metal–ligand bond covalence by offering a coordination environment in which π-electron density is shifted multi-directionally from amido-donors to Cr^{III} and from Cr^{III} to pyridine-acceptors. This seems indeed to be the case, and our investigation points to a substantially lowered Racah *B* parameter, which gives rise to the first NIR-II emissive Cr^{III} complex.

Results and Discussion

Synthesis, Structure and Electrochemistry

The tridentate ligand precursor, 3,6-di-*tert*-butyl-1,8-di(-pyridine-2-yl)-carbazole (H-dpc), was synthesized following a known procedure.[30] This compound was deprotonated with lithium diisopropylamide (LDA), and subsequent addition of $CrCl_2$ (99.99% purity) and halide exchange with potassium hexafluorophosphate under air resulted in the formation of $[Cr(dpc)_2](PF_6)$ as a dark red solid in 41% yield (Scheme 1). The new complex is stable under both acidic and basic conditions (Figure S4/S5).

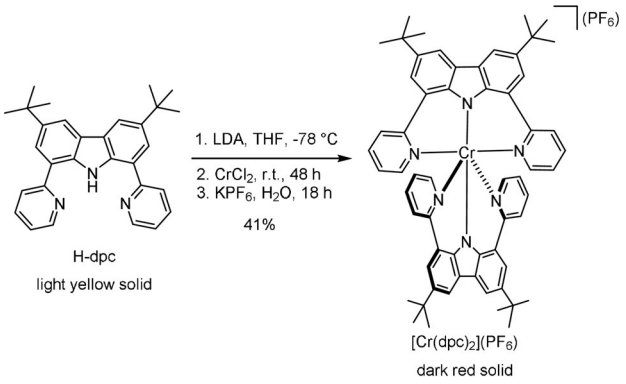

Scheme 1. Synthesis of the new chromium(III) complex, $[Cr(dpc)_2](PF_6)$.

Red colored single crystals of $[Cr(dpc)_2](PF_6)\cdot 2.5(C_2H_4Cl_2)$ for an X-ray diffraction study were obtained by slow vapor diffusion of *n*-hexane into a saturated solution of $[Cr(dpc)_2](PF_6)$ in dichloroethane at 4 °C. The structure analysis revealed the expected mononuclear chromium(III) complex cation bearing two dpc ligands, which is shown in Figure 3. The complex cation features close to octahedral geometry for the six bound nitrogen atoms around the chromium(III) center. The N(amido)-Cr-N(amido) angle is 173.69(8)°, and the N(pyridine)-Cr-N(pyridine) angles are 173.16(7) and 173.66(7)°. These bond angles are very similar to those reported for $[Cr(ddpd)_2]^{3+}$.[5–6] The Cr-N(amido) bond lengths (1.962(3) and 1.969(2) Å) are shorter than the Cr-N(pyridine) bonds (2.109(3)-2.133(2) Å), which is compatible with the more covalent nature of the Cr-N(amido) bonds. A recent study of lithium amides revealed significant covalent Li–N bonding character, and comparatively short bond distances.[31] The two pyridine rings of a given dpc ligand are tilted from the plane of the central carbazole ring in such a way that the tridentate ligand adopts a helical twist compatible with *P* and *M* chirality according to Cahn-Ingold-Prelog notation.[32] As previously reported for $[Cr(dqp)_2]^{3+}$ [6] and $[Cr(ddpd)_2]^{3+}$,[33] the homochiral *PP* and *MM* pairs are more stable than the heterochiral *PM* assembly in the chromium(III) complex, which therefore exists as a pair of

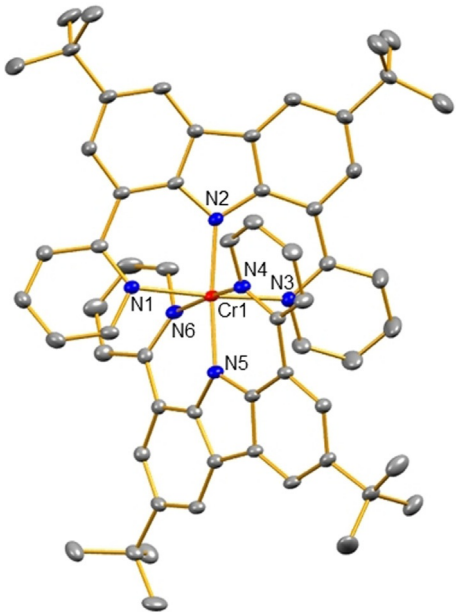

Figure 3. Molecular structure of $[Cr(dpc)_2]^+$ in $[Cr(dpc)_2](PF_6)\cdot 2.5(C_2H_4Cl_2)$ (H atoms, the counter ion and solvent molecules are omitted for clarity, 50% probability ellipsoids). Selected bond angles (°) and bond distances (Å): N2-Cr1-N5, 173.69(8); N1-Cr1-N3, 173.66(7); N4-Cr1-N6, 173.16(7); Cr1-N2, 1.969(2); Cr1-N5, 1.962(3); Cr1-N1, 2.133(2); Cr1-N3, 2.115(3); Cr1-N4, 2.109(3); Cr1-N6, 2.133(2). CCDC 2082071 ($[Cr(dpc)_2](PF_6)\cdot 2.5(C_2H_4Cl_2)$) contains the supplementary crystallographic data for this paper. These data can be obtained free of charge from the Cambridge Crystallographic Data Centre.

PP-$[Cr(dpc)_2]^+$/*MM*-$[Cr(dpc)_2]^+$ enantiomers in the crystal structure.

The uncommon electronic structure of $[Cr(dpc)_2]^+$ readily manifests in cyclic voltammetry (Figure 4a), where the first reduction event is observable at −1.51 V vs. $Fc^{+/0}$ (−0.88 V vs. NHE),[34] cathodically shifted by ca. 1.0 V relative to $[Cr(tpy)_2]^{3+}$ and at ca. 0.4 V more negative potential than in $[Cr(ddpd)_2]^{3+}$.[5] The electron-poor pyridine ligands of fused-five-membered tpy chelates in $[Cr(tpy)_2]^{3+}$ lead to a situation in which the first reduction process is ligand-centered, occurring at + 0.1 V vs. NHE to give $[Cr^{III}(tpy^{\cdot -})(tpy)]^{2+}$ with no trace of Cr^{II}.[35a] On the other hand, $[Cr(ddpd)_2]^{3+}$ with its fused six-membered electron-rich ddpd chelates exhibits metal-centered reduction at −0.48 V vs. NHE to give the spin-crossover compound $[Cr^{II}(ddpd)_2]^{2+}$.[35b] The electron-rich character of our anionic dpc ligand, combined with its six-membered chelate rings suggest an analogous metal-centered reduction to give $[Cr^{II}(dpc)_2]^0$, but cathodically shifted with respect to $[Cr(ddpd)_2]^{3+}$ due to the high electron density at the metal center. The latter characteristics furthermore facilitate the observation of a $Cr^{IV/III}$ redox couple at 0.46 V vs. $Fc^{+/0}$ (−0.17 V vs. NHE), which does not seem to be detectable for the other complexes in Figure 1. An additional wave at 0.78 V vs. $Fc^{+/0}$ in Figure 4a is attributable to ligand oxidation, because a similar (though less reversible) wave (due to possible deprotonation) is observed for the ligand precursor H-dpc (Figure S6). See SI page S9 for a further discussion regarding the assignment of the individual redox waves.

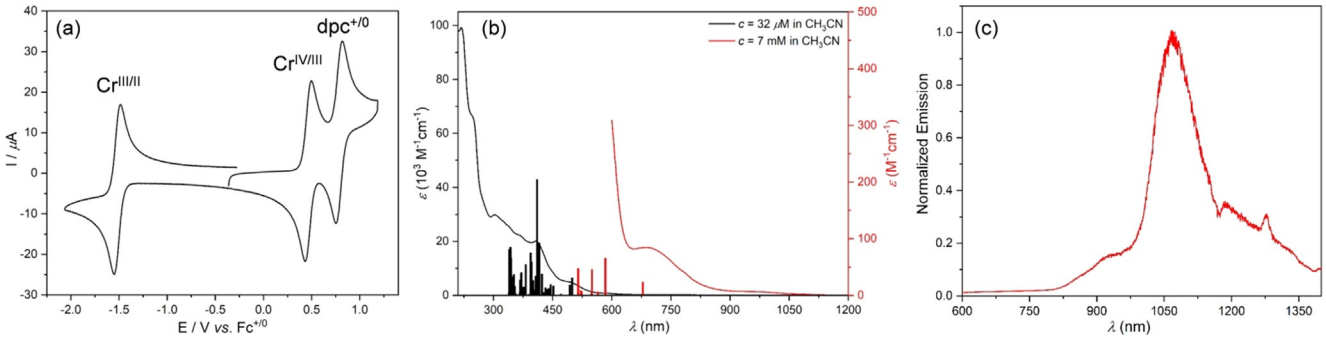

Figure 4. (a) Cyclic voltammogram of 1 mM $[Cr(dpc)_2](PF_6)$ in acetonitrile with 0.1 M ($^nBu_4N$)(PF_6) as supporting electrolyte, recorded at a scan rate of 100 mV s^{-1}. (The $Fc^{+/0}$ potential corresponds to 0.63 V vs. NHE).[34] (b) UV/Vis absorption spectrum of $[Cr(dpc)_2](PF_6)$ in acetonitrile at 20 °C (black trace). The red trace shows the long-wavelength part of this spectrum on a magnified ε-scale (right *y*-axis, recorded on a more concentrated solution, see inset). The vertical black and red bars mark the energies of DFT-calculated vertical transitions, the heights of these bars reflect relative oscillator strengths. The heights of the vertical red bars were multiplied by a factor of 10 relative to the vertical black bars. (c) Luminescence spectrum of $[Cr(dpc)_2](PF_6)$ in acetonitrile at 77 K, obtained after excitation at 450 nm.

UV/Vis Absorption Spectroscopy

The UV/Vis absorption spectrum of $[Cr(dpc)_2]^+$ in acetonitrile (Figure 4b) exhibits ligand-centered π-π* absorption bands between 220 and 330 nm with molar extinction coefficients (ε) exceeding 30000 M^{-1}cm^{-1}. The spectral range between 330 and 450 nm is dominated by (spin-allowed) ligand-to-metal charge transfer (LMCT) absorptions according to time-dependent DFT calculations (Tables S2-S3), along with some metal-to-ligand charge transfer (MLCT) and (weaker) metal-centered (MC) absorption features. Given the anionic nature of the amido donor group, the observation of ^{4}LMCT absorptions is unsurprising, and based on the electrochemical data in Figure 4a one would expect some of them to fall into the visible range near 2.4 eV. At 500 nm there is a distinct absorption band ($\varepsilon = 4660$ M^{-1}cm^{-1}) which, according to the TD-DFT calculations, is attributable to an intraligand charge transfer (ILCT) between carbazole and pyridine units. The presence of all these comparatively intense charge transfer (CT) absorption bands makes the observation of the parity-forbidden MC absorptions difficult. The absorption band at 521 nm ($\varepsilon = 3000$ M^{-1}cm^{-1}) contains significant $^4A_2 \rightarrow {}^4T_2$ character according to the TD-DFT calculations. For comparison, in the $[Cr(ddpd)_2]^{3+}$ and $[Cr(dqp)_2]^{3+}$ complexes the $^4T_2$ absorption maximum appears at 434 and 401 nm, respectively.[5,6] A red-shift of the $^4A_2 \rightarrow {}^4T_2$ absorption band in $[Cr(dpc)_2]^+$ is expected, as the amido π-donor unit of dpc destabilizes the t_{2g}-like metal orbitals and thereby weakens the ligand field compared to the pyridine and quinoline π-acceptor units of ddpd and dqp.

Aiming to detect the spin-forbidden transitions from the $^4A_2$ ground state to the ^{2}E and $^2T_1$ excited states, an absorption spectrum of a more concentrated solution of $[Cr(dpc)_2](PF_6)$ in acetonitrile was recorded (red trace in Figure 4b), but instead of the anticipated rather narrow spectral features, two comparatively broad bands were observable. The first of these two bands peaks at 690 nm with $\varepsilon = 84$ M^{-1}cm^{-1} and corresponds to a spin-forbidden ^{2}LMCT according to TD-DFT. The second band around 970 nm is yet an order of magnitude weaker ($\varepsilon = 6$ M^{-1}cm^{-1}) and will be discussed below alongside luminescence data.

Photoluminescence

Following excitation of $[Cr(dpc)_2](PF_6)$ at 450 nm in acetonitrile at 77 K, the luminescence spectrum in Figure 4c was recorded. The emission peak is at 1067 nm, flanked by a tail extending to 1350 nm and a weaker shoulder at shorter wavelengths. The excitation spectrum of the emission at 1067 nm matches the absorption spectrum between 350 and 550 nm well (Figure S12). Pulsed excitation at 350 nm reveals a bi-exponential decay of the luminescence signal at 1067 nm (Figure S11) with lifetimes (τ) of 1.4 μs (88 %) and 6.3 μs (12 %). Three facts seem particularly noteworthy concerning this emission: (i) its long wavelength compared to the other complexes from Figure 1 for which $^2E \rightarrow {}^4A_2$ luminescence typically peaked between 727 and 778 nm; (ii) its comparatively broad spectral bandwidth; (iii) its relatively short lifetime, falling into the single-digit microsecond regime.

The long emission wavelength is compatible with the UV/Vis absorption spectrum showing its lowest absorption band around 970 nm with $\varepsilon = 6$ M^{-1}cm^{-1}, and therefore seems in line with a ^{2}E-like emission of $[Cr(dpc)_2]^+$. The uncommon emission spectral bandwidth could have its origin in the energetic proximity of the ^{2}LMCT state (absorption maximum at 690 nm, but extending to nearly 900 nm) and consequent admixture of LMCT character to the emissive excited state. It seems plausible that this contributes to the width of the emission band in Figure 4c, because the LMCT character implies distortions along additional nuclear coordinates.

Similarly, it seems plausible that the comparatively short luminescence lifetime of $[Cr(dpc)_2]^+$ is related to LMCT admixture to the ^{2}E-like emission, introducing more parity-allowed character to the resulting electronic transition and thereby enhancing the radiative decay rate. The determination of luminescence quantum yields on frozen solutions at 77 K are technically very demanding and were not performed in the current study, hence we cannot exclude that non-radiative relaxation contributes substantially to the emission decay even at cryogenic temperature.

No luminescence was detectable at room temperature, using experimental conditions under which we were able to

detect the weak luminescence emitted by $[Cr(tpy)_2]^{3+}$. This indicates that the luminescence quantum yield of $[Cr(dpc)_2]^+$ under these conditions is below 0.00089 % (Figure 1c). This could be related to the possibility that the emission transition is not a pure spin-flip, but contains some LMCT character that entails more significant excited-state distortions than in common Cr^{III} polypyridines. Furthermore, the energy gap of ca. 9400 cm^{-1} between the emissive excited state and the electronic ground state in $[Cr(dpc)_2]^+$ merely corresponds to approximately 3 quanta of C–H stretching vibrations (with an approximate frequency of ca. 3000 cm^{-1}). Consequently, electronic-vibrational coupling to such high-frequency modes could readily entail efficient nonradiative relaxation, even in a scenario in which overall excited-state distortion is relatively modest. In $[Cr(ddpd)_2]^{3+}$, the aromatic C–H bonds of the pyridine units contributed most to the nonradiative excited-state decay,[8] and it seems plausible that this is also the case for $[Cr(dpc)_2]^+$.

Ligand Field Parameters

The optical spectroscopic properties of Cr^{3+} doped inorganic materials and molecular complexes of Cr^{III} are traditionally analyzed in the framework of ligand field theory. The two key figures of merit are the ligand field parameter 10 Dq and the Racah *B* parameter, which are measures for the magnitude of the energetic splitting between metal-based t_{2g}- and e_g-orbitals and for metal–ligand bond covalence. Despite the fact that the symmetry of $[Cr(dpc)_2]^+$ is lower than octahedral and even though very limited information concerning the energies of MC states is available for this compound, we consider a brief analysis in terms of ligand field theory useful, particularly because this will allow comparison to previously investigated chromium(III) compounds. As noted above, most MC states are masked by intense charge transfer transitions in the UV/Vis absorption spectrum of $[Cr(dpc)_2]^+$, but the $^4A_2 \rightarrow {}^4T_2$ transition is calculated to occur at 521 nm, hence 10 Dq is estimated to roughly 19200 cm^{-1} (equation S1). Since the $^2E \rightarrow {}^4T_2$ emission peaks at 1067 nm, we approximate the energy of the ^2E state as 9400 cm^{-1}. Lacking further experimental information about MC state energies in $[Cr(dpc)_2]^+$, we assume that the relationship $C = 4 \cdot B$ is applicable, which represents an approximation made by many textbooks.[36] *C* is an additional electron-electron repulsion parameter required to calculate the energy of the ^2E state (equation S2), and using the above-mentioned relationship, a value of 470 cm^{-1} is obtained for the Racah *B* parameter. For the previously investigated $[Cr(ddpd)_2]^{3+}$ and $[Cr(dqp)_3]^{3+}$ compounds *B*-values of 760 cm^{-1} and 660 cm^{-1} have been reported (Table 1),[5,9b] falling into the typical range of Racah *B* parameters of Cr^{3+} doped oxides, fluorides, and chlorides (600–750 cm^{-1}).[37]

Given the various approximations and experimental limitations outlined above, our own estimate for *B* is undoubtedly associated with considerable uncertainty, yet it seems clear that the value of 470 cm^{-1} stands out. Even if we assume a relationship of $C = 3.2 \cdot B$ (as was the case for $[Cr(ddpd)_2]^{3+}$),[5] we obtain $B = 550\ cm^{-1}$, which remains significantly lower than all other Racah *B* parameter summarized in Table 1. It follows that the nephelauxetic parameter β, which corresponds to the ratio of *B*-values in a given complex and in the corresponding free ion,[12] is in the range of 0.5 to 0.6 for $[Cr(dpc)_2]^+$ (the *B*-value for the free Cr^{3+} ion is 918 cm^{-1},[11] see above). Within the framework of the simplifications made for this analysis, notably the assumption of octahedral symmetry, this implies that the average metal–ligand bond in $[Cr(dpc)_2]^+$ has unusually strong covalent character.[41]

Table 1: Ligand field parameters for selected molecular Cr^{III} complexes and Cr^{3+} doped inorganic materials.[a]

Compound	10 Dq [cm^{-1}]	*B* [cm^{-1}]
$[Cr(ddpd)_2]^{3+}$[b]	22900	760
$[Cr(dqp)_3]^{3+}$[c]	24925	660
$[Cr(phen)_3]^{3+}$[d]	22075	780
$[Cr(dpc)_2]^{+}$[e]	19200	470
Cr^{3+}:α-Al_2O_3 (ruby)[f]	18000	650
Cr^{3+}:$Y_3Al_5O_{12}$[f]	16400	650
Cr^{3+}:$LiCaAlF_6$[f]	16075	750
Cr^{3+}:$Cs_2NaScCl_6$[g]	12800	600
Cr^{3+}:$Cs_2NaScYCl_6$[h]	12800	600

[a] 10 Dq-values rounded to increments of 25 cm^{-1}, *B*-values rounded to increments of 10 cm^{-1}. [b] From ref. [5]; [c] from ref. [9b]; [d] from ref. [38]; [e] this work; [f] from ref. [37]; [g] from ref. [39]; [h] from ref. [40].

Conclusion

Previously reported spin-flip emissions of chromium(III) complexes were typically in the range between 727 and 778 nm, but the NIR-II luminescence measured for $[Cr(dpc)_2]^+$ at 1067 nm is unprecedented to the best of our knowledge. This strong red-shift seems to be the consequence of unusually strong metal–ligand bond covalence, which weakens the mutual repulsion between d-electrons in the emissive excited state, thereby lowering its energy such that NIR-II luminescence results. An energetically low-lying ^{2}LMCT excited state furthermore influences the luminescence of $[Cr(dpc)_2]^+$, manifesting in an overall excited-state distortion that is more substantial than in previously explored compounds and leading to a comparatively broad emission band shape. As a further consequence of this LMCT admixture and the lowered ^2E energy, nonradiative relaxation from the emissive excited state is more efficient than in previously investigated Cr^{III} polypyridines.

The combination of a π-donating amido unit flanked by two π-accepting pyridine moieties in a bite-angle optimized, six-membered terdentate chelate ligand enables the coordination of Cr^{III} in a manner that π-electron density can shift from the ligands to the metal in axial direction, whereas in the equatorial plane π-electron density flows from the metal towards the ligands. These combined push- and pull-interactions can act strongly on the spectroscopically relevant dπ-electrons of Cr^{III}, and this seems to be the key to inducing a strong nephelauxetic effect and the ensuing highly uncommon photophysical properties. Thus, our study unravels a new design principle for luminescent Cr^{III} compounds; whilst prior

studies have focused on maximizing ligand field strength and on optimizing ligand bite angles, our work demonstrates that increasing the metal–ligand bond covalence through combined π-donor and π-acceptor interactions allows emission color tuning and can lead to NIR-II luminescence. Moreover, the inert and chiral nature of the $[Cr(dpc)_2]^+$ chromophore opens perspectives for the induction of circularly polarized emission in the NIR-II domain while using an abundant 3d-metal.

These insights complement recent ground-breaking discoveries in the photophysics and the photochemistry of complexes with other first-row transition metals, including $V^{II/III}$,[23,42] Mn^{IV},[43] Fe^{II},[25] Fe^{III},[44] Co^{III},[45] Ni^{II},[46] and Cu^{I}.[22c,47] It seems that much fundamental work is yet needed to fully elucidate the potential of 3d-metals for applications in luminophores, light harvesting, sensing, photocatalysis and beyond.

Acknowledgements

This work was supported by the Swiss National Science Foundation through grant numbers 200021 178760 and 200020 178758. The present project was supported by the National Research Fund, Luxembourg (PhD grant 14583224 to B.P.).

Conflict of Interest

The authors declare no conflict of interest.

Keywords: chelates · chromium · luminescence · photophysics · UV/Vis spectroscopy

[1] A. Hauser, C. Reber, *Struct. Bonding (Berlin)* **2016**, *172*, 291 – 312.
[2] M. Milos, A. Hauser, *J. Lumin.* **2013**, *133*, 15 – 20.
[3] a) R. Farran, L. Le-Quang, J. M. Mouesca, V. Maurel, D. Jouvenot, F. Loiseau, A. Deronzier, J. Chauvin, *Dalton Trans.* **2019**, *48*, 6800 – 6811; b) A. D. Kirk, G. B. Porter, *J. Phys. Chem.* **1980**, *84*, 887 – 891.
[4] N. Serpone, M. A. Jamieson, M. S. Henry, M. Z. Hoffman, F. Bolletta, M. Maestri, *J. Am. Chem. Soc.* **1979**, *101*, 2907 – 2916.
[5] S. Otto, M. Grabolle, C. Förster, C. Kreitner, U. Resch-Genger, K. Heinze, *Angew. Chem. Int. Ed.* **2015**, *54*, 11572 – 11576; *Angew. Chem.* **2015**, *127*, 11735 – 11739.
[6] J. R. Jiménez, B. Doistau, C. M. Cruz, C. Besnard, J. M. Cuerva, A. G. Campagna, C. Piguet, *J. Am. Chem. Soc.* **2019**, *141*, 13244 – 13252.
[7] a) S. Otto, A. M. Nauth, E. Emilov, N. Scholz, A. Friedrich, U. Resch-Genger, S. Lochbrunner, T. Opatz, K. Heinze, *ChemPhotoChem* **2017**, *1*, 344 – 349; b) S. Otto, N. Scholz, T. Behnke, U. Resch-Genger, K. Heinze, *Chem. Eur. J.* **2017**, *23*, 12131 – 12135; c) C. Förster, M. Dorn, T. Reuter, S. Otto, G. Davarci, T. Reich, L. Carrella, E. Rentschler, K. Heinze, *Inorganics* **2018**, *6*, 86; d) S. Otto, M. Dorn, C. Förster, M. Bauer, M. Seitz, K. Heinze, *Coord. Chem. Rev.* **2018**, *359*, 102 – 111; e) S. Otto, J. P. Harris, K. Heinze, C. Reber, *Angew. Chem. Int. Ed.* **2018**, *57*, 11069 – 11073; *Angew. Chem.* **2018**, *130*, 11236 – 11240.
[8] C. Wang, S. Otto, M. Dorn, E. Kreidt, J. Lebon, L. Srsan, P. Di Martino-Fumo, M. Gerhards, U. Resch-Genger, M. Seitz, K. Heinze, *Angew. Chem. Int. Ed.* **2018**, *57*, 1112 – 1116; *Angew. Chem.* **2018**, *130*, 1125 – 1130.
[9] a) J. R. Jiménez, B. Doistau, C. Besnard, C. Piguet, *Chem. Commun.* **2018**, *54*, 13228 – 13231; b) J.-R. Jiménez, M. Poncet, B. Doistau, C. Besnard, C. Piguet, *Dalton Trans.* **2020**, *49*, 13528 – 13532; c) J.-R. Jiménez, M. Poncet, S. Míguez-Lago, S. Grass, J. Lacour, C. Besnard, J. M. Cuerva, A. G. Campaña, C. Piguet, *Angew. Chem. Int. Ed.* **2021**, *60*, 10095 – 10102; *Angew. Chem.* **2021**, *133*, 10183 – 10190..
[10] S. Treiling, C. Wang, C. Förster, F. Reichenauer, J. Kalmbach, P. Boden, J. Harris, L. Carrella, E. Rentschler, U. Resch-Genger, C. Reber, M. Seitz, M. Gerhards, K. Heinze, *Angew. Chem. Int. Ed.* **2019**, *58*, 18075 – 18085; *Angew. Chem.* **2019**, *131*, 18243 – 18253.
[11] Y. Tanabe, S. Sugano, *J. Phys. Soc. (Japan)* **1954**, *9*, 766 – 779.
[12] a) C. K. Jorgensen, *Discuss. Faraday Soc.* **1958**, 110 – 115; b) C. E. Schäffer, C. K. Jorgensen, *J. Inorg. Nucl. Chem.* **1958**, *8*, 143 – 148.
[13] L. A. Büldt, O. S. Wenger, *Chem. Sci.* **2017**, *8*, 7359 – 7367.
[14] a) M. Ibrahim-Ouali, F. Dumur, *Molecules* **2019**, *24*, 1412; b) H. Xiang, J. Cheng, X. Ma, X. Zhou, J. J. Chruma, *Chem. Soc. Rev.* **2013**, *42*, 6128 – 6185.
[15] H. Q. Ye, Z. Li, Y. Peng, C. C. Wang, T. Y. Li, Y. X. Zheng, A. Sapelkin, G. Adamopoulos, I. Hernández, P. B. Wyatt, W. P. Gillin, *Nat. Mater.* **2014**, *13*, 382 – 386.
[16] A. Baride, J. M. Meruga, C. Douma, D. Langerman, G. Crawford, J. J. Kellar, W. M. Cross, P. S. May, *RSC Adv.* **2015**, *5*, 101338 – 101346.
[17] a) A. Foucault-Collet, K. A. Gogick, K. A. White, S. Villette, A. Pallier, G. Collet, C. Kieda, T. Li, S. J. Geib, N. L. Rosi, S. Petoud, *Proc. Natl. Acad. Sci. USA* **2013**, *110*, 17199 – 17204; b) S. V. Eliseeva, J.-C. G. Bünzli, *Chem. Soc. Rev.* **2010**, *39*, 189 – 227.
[18] K. Tuong Ly, R.-W. Chen-Cheng, H.-W. Lin, Y.-J. Shiau, S.-H. Liu, P.-T. Chou, C.-S. Tsao, Y.-C. Huang, Y. Chi, *Nat. Photonics* **2017**, *11*, 63 – 68.
[19] Q. Zhao, C. Huang, F. Li, *Chem. Soc. Rev.* **2011**, *40*, 2508 – 2524.
[20] a) B. Li, M. Zhao, L. Feng, C. Dou, S. Ding, G. Zhou, L. Lu, H. Zhang, F. Chen, X. Li, G. Li, S. Zhao, C. Jiang, Y. Wang, D. Zhao, Y. Cheng, F. Zhang, *Nat. Commun.* **2020**, *11*, 3102; b) Q. Yang, Z. Hu, S. Zhu, R. Ma, H. Ma, Z. Ma, H. Wan, T. Zhu, Z. Jiang, W. Liu, L. Jiao, H. Sun, Y. Liang, H. Dai, *J. Am. Chem. Soc.* **2018**, *140*, 1715 – 1724; c) M. Schulze, A. Steffen, F. Würthner, *Angew. Chem. Int. Ed.* **2015**, *54*, 1570 – 1573; *Angew. Chem.* **2015**, *127*, 1590 – 1593.
[21] F. Ding, Z. Chen, W. Y. Kim, A. Sharma, C. Li, Q. Ouyang, H. Zhu, G. Yang, Y. Sun, J. S. Kim, *Chem. Sci.* **2019**, *10*, 7023 – 7028.
[22] a) O. S. Wenger, *J. Am. Chem. Soc.* **2018**, *140*, 13522 – 13533; b) C. Förster, K. Heinze, *Chem. Soc. Rev.* **2020**, *49*, 1057 – 1070; c) M. Gernert, L. Balles-Wolf, F. Kerner, U. Müller, A. Schmiedel, M. Holzapfel, C. M. Marian, J. Pflaum, C. Lambert, A. Steffen, *J. Am. Chem. Soc.* **2020**, *142*, 8897 – 8909.
[23] M. Dorn, J. Kalmbach, P. Boden, A. Päpcke, S. Gómez, C. Förster, F. Kuczelinis, L. M. Carrella, L. Büldt, N. Bings, E. Rentschler, S. Lochbrunner, L. González, M. Gerhards, M. Seitz, K. Heinze, *J. Am. Chem. Soc.* **2020**, *142*, 7947 – 7955.
[24] J. K. McCusker, *Science* **2019**, *363*, 484 – 488.
[25] J. D. Braun, I. B. Lozada, C. Kolodziej, C. Burda, K. M. E. Newman, J. van Lierop, R. L. Davis, D. E. Herbert, *Nat. Chem.* **2019**, *11*, 1144 – 1150.
[26] J. D. Braun, I. B. Lozada, D. E. Herbert, *Inorg. Chem.* **2020**, *59*, 17746 – 17757.
[27] S. Mukherjee, D. E. Torres, E. Jakubikova, *Chem. Sci.* **2017**, *8*, 8115 – 8126.
[28] M. Moser, B. Wucher, D. Kunz, F. Rominger, *Organometallics* **2007**, *26*, 1024 – 1030.

[29] O. S. Wenger, *Chem. Eur. J.* **2019**, *25*, 6043 – 6052.
[30] M. S. Mudadu, A. N. Singh, R. P. Thummel, *J. Org. Chem.* **2008**, *73*, 6513 – 6520.
[31] F. Engelhardt, C. Maaß, D. M. Andrada, R. Herbst-Irmer, D. Stalke, *Chem. Sci.* **2018**, *9*, 3111 – 3121.
[32] R. S. Cahn, C. Ingold, V. Prelog, *Angew. Chem. Int. Ed. Engl.* **1966**, *5*, 385 – 415; *Angew. Chem.* **1966**, *78*, 413 – 447.
[33] C. Dee, F. Zinna, W. R. Kitzmann, G. Pescitelli, K. Heinze, L. Di Bari, M. Seitz, *Chem. Commun.* **2019**, *55*, 13078 – 13081.
[34] V. V. Pavlishchuk, A. W. Addison, *Inorg. Chim. Acta* **2000**, *298*, 97 – 102.
[35] a) C. C. Scarborough, K. M. Lancaster, S. DeBeer, T. Weyhermüller, S. Sproules, K. Wieghardt, *Inorg. Chem.* **2012**, *51*, 3718 – 3732; b) P. M. Becker, C. Förster, L. M. Carella, P. Boden, D. Hunger, J. van Slageren, M. Gerhards, E. Rentschler, K. Heinze, *Chem. Eur. J.* **2020**, *26*, 7199 – 7204.
[36] P. W. Atkins, T. L. Overton, J. P. Rourke, M. T. Weller, F. A. Armstrong, *Shriver and Atkins' Inorganic Chemistry*, Oxford University Press, **2000**.
[37] M. Back, J. Ueda, H. Hua, S. Tanabe, *Chem. Mater.* **2021**, *33*, 3379 – 3385.
[38] B. Doistau, G. Collet, E. A. Bolomey, V. Sadat-Noorbakhsh, C. Besnard, C. Piguet, *Inorg. Chem.* **2018**, *57*, 14362 – 14373.
[39] O. S. Wenger, H. U. Güdel, *J. Chem. Phys.* **2001**, *114*, 5832 – 5841.
[40] R. W. Schwartz, *Inorg. Chem.* **1976**, *15*, 2817 – 2822.
[41] S. K. Singh, J. Eng, M. Atanasov, F. Neese, *Coord. Chem. Rev.* **2017**, *344*, 2 – 25.
[42] R. D. Dill, R. I. Portillo, S. G. Shepard, M. P. Shores, A. K. Rappé, N. H. Damrauer, *Inorg. Chem.* **2020**, *59*, 14706 – 14715.
[43] J. P. Harris, C. Reber, H. E. Colmer, T. A. Jackson, A. P. Forshaw, J. M. Smith, R. A. Kinney, J. Telser, *Can. J. Chem.* **2017**, *95*, 547 – 552.
[44] K. S. Kjær, N. Kaul, O. Prakash, P. Chábera, N. W. Rosemann, A. Honarfar, O. Gordivska, L. A. Fredin, K. E. Bergquist, L. Häggström, T. Ericsson, L. Lindh, A. Yartsev, S. Styring, P. Huang, J. Uhlig, J. Bendix, D. Strand, V. Sundström, P. Persson, R. Lomoth, K. Wärnmark, *Science* **2019**, *363*, 249 – 253.
[45] a) S. Kaufhold, N. W. Rosemann, P. Chábera, L. Lindh, I. B. Losada, J. Uhlig, T. Pascher, D. Strand, K. Wärnmark, A. Yartsev, P. Persson, *J. Am. Chem. Soc.* **2021**, *143*, 1307 – 1312; b) A. K. Pal, C. F. Li, G. S. Hanan, E. Zysman-Colman, *Angew. Chem. Int. Ed.* **2018**, *57*, 8027 – 8031; *Angew. Chem.* **2018**, *130*, 8159 – 8163.
[46] a) Y.-S. Wong, M.-C. Tang, M. Ng, V. W.-W. Yam, *J. Am. Chem. Soc.* **2020**, *142*, 7638 – 7646; b) S. I. Ting, S. Garakyaraghi, C. M. Taliaferro, B. J. Shields, G. D. Scholes, F. N. Castellano, A. G. Doyle, *J. Am. Chem. Soc.* **2020**, *142*, 5800 – 5810; c) O. S. Wenger, *Chem. Eur. J.* **2021**, *27*, 2270 – 2278; d) R. Lauenstein, S. L. Mader, H. Derondeau, O. Z. Esezobor, M. Block, A. J. Römer, C. Jandl, E. Riedle, V. Kaila, J. Hauer, E. Thyrhaug, C. R. Hess, *Chem. Sci.* **2021**, *12*, 7521 – 7532.
[47] a) R. Hamze, J. L. Peltier, D. Sylvinson, M. Jung, J. Cardenas, R. Haiges, M. Soleilhavoup, R. Jazzar, P. I. Djurovich, G. Bertrand, M. E. Thompson, *Science* **2019**, *363*, 601 – 606; b) M. Heberle, S. Tschierlei, N. Rockstroh, M. Ringenberg, W. Frey, H. Junge, M. Beller, S. Lochbrunner, M. Karnahl, *Chem. Eur. J.* **2017**, *23*, 312 – 319.

Manuscript received: May 12, 2021
Accepted manuscript online: June 14, 2021
Version of record online: July 12, 2021

